



FPGA-based Implementation of Multiple PHY Layers of IEEE 802.15.4 Targeting SDR Platform

Albdelbassat Massouri, Tanguy Risset

► To cite this version:

Albdelbassat Massouri, Tanguy Risset. FPGA-based Implementation of Multiple PHY Layers of IEEE 802.15.4 Targeting SDR Platform. SDR-WinnComm, Apr 2014, Schaumburg, Illinois, United States. hal-01005317

HAL Id: hal-01005317

<https://inria.hal.science/hal-01005317>

Submitted on 12 Jun 2014

HAL is a multi-disciplinary open access archive for the deposit and dissemination of scientific research documents, whether they are published or not. The documents may come from teaching and research institutions in France or abroad, or from public or private research centers.

L'archive ouverte pluridisciplinaire **HAL**, est destinée au dépôt et à la diffusion de documents scientifiques de niveau recherche, publiés ou non, émanant des établissements d'enseignement et de recherche français ou étrangers, des laboratoires publics ou privés.

FPGA-based Implementation of Multiple PHY Layers of IEEE 802.15.4 Targeting SDR Platform

Abdelbassat MASSOURI and Tanguy RISSET
Université de Lyon, INRIA,
INSA-Lyon, CITI-INRIA, F-69621, Villeurbanne, France
firstname.lastname@inria.fr

Abstract—While SDR platforms become more and more accessible to a large community of researchers with affordable prices, open source FPGA-based implementation of wireless communication systems are still not available. This paper presents an open source FPGA-based design of IEEE 802.15.4 PHY Layers developed in the context of a new SDR testbed named FIT/CorteXlab. We propose a VHDL implementation of the three available options of the IEEE 802.15.4 physical layer parametrized and easily reconfigurable. We have validated our design on *Nutaq* platform which combines *Xilinx Virtex-6* FPGA and tunable *Radio420x* RF transceiver. A tutorial style approach is adopted to describe the multiple PHY Layers of both the baseband TX and RX IPs of IEEE 802.15.4 standard. More focus is given to the symbol timing/carrier recovery and considerations for FPGA implementation are outlined. The IPs presented here will participate to the building of an open source hardware SDR library similar to GNU radio but targeted to FPGA-based platforms.

Keywords—IEEE 802.15.4, Zigbee, Software Defined Radio, Cognitive Radio, FPGA.

I. INTRODUCTION

Software Defined Radio (SDR) has been identified by Mitola many years ago [8], but the SDR technology has been accessible at reasonable price only recently. Based on this technological shift, the advent cognitive radio networks is a major research challenge as it has been pointed by NSF in 2009 [16]. One of the recommendations of this report concerned the lack of cognitive radio testbeds and the urge to “develop a set of cognitive networking test-beds that can be used to evaluate cognitive networks at various stages of their development”.

While open source software is widely used for cooperative academic project, open source hardware is still hard to find. OpenCores [13] is one of the most well known organization providing open source VHDL, but it mainly provides processors because it does not target a particular application domain. Providing dedicated IPs for a particular application domain, here SDR, will help in building a common source repository. An example of such *closed* community is the *reconfigurable video coding standard* framework [7] supported by MPEG to help in developing portable video coding applications. Given that cognitive radio is foreseen as a major innovative field in the next ten years, it will need a similar effort to help new waveform deployment on various SDR architectures.

However, modern wireless technologies based on OFDM (Orthogonal Frequency Division Multiplexing) such as WiFi or LTE-Advanced suffer from a major disadvantage: they require a high computing power. For instance, LTE-Advanced is suppose to require 40Gops with a power consumption of less than 1 Watt. Hence, dedicated hardware IPs have to be used to meet the computing power required. This explains the fact that no open-source library exists so far for this domain: dedicated IPs are very specific to their target protocol and moreover their design is very time-consuming. This situation should change as it will become mandatory to provide re-usable code for software defined radio as the technology is mature now. The growing use of software radio application will improve the development of open source hardware design for digital signal processing and we contribute, with the design presented here, to this developpement

In section II, we briefly review existing testbed that can be used for SDR application and we present the FIT/CorteXlab testbed. Section III presents the multiple PHY layers that we provide according to the IEEE 802.15.4 standard. Finally, the performance of the implementation of our design on Virtex 6 FPGA is presented.

II. SDR TESTBED

Recently, many testbeds have been built in the field of wireless communications, targeted to wireless sensor or Wifi networks. However, only a few large-scale testbeds have been developed in the SDR and cognitive radio field (CREW [15], TRIAL and CORNET [11] are the main ones).

We are currently building a new cognitive radio testbed in Lyon named CorteXlab (see figure 1), as part of the Future Internet of Things [4] french funding. Cognitive radio nodes together with wireless sensor nodes will be deployed in a electromagnetically isolated room so as to bring radio propagation under control. The testbed will be open to the scientific community within two years and will allow academics and industrials to conduct real-life cognitive radio experiments. Nodes will be remotely programmable just as if users had them on their desk.

In [3], a survey of existing SDR architectures highlights the fact that there is currently no accepted common execution model for SDR platform. However, we believe that the use of a powerful FPGA for baseband processing implementation

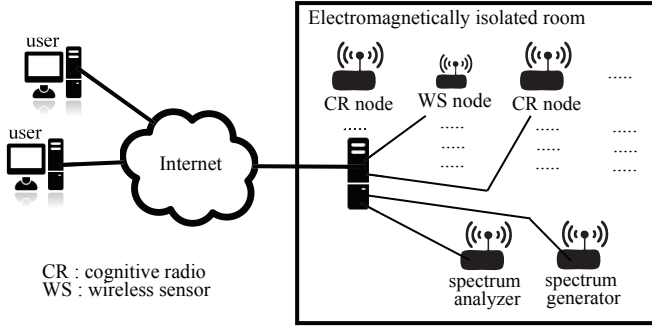


Fig. 1: Hardware/software requirements for the CorteXlab cognitive radio node (figure from [3]).

is currently the most promising approach for prototypes. In CorteXlab, two types of nodes have been deployed: USRP nodes from National Instrument [10] and picoSDR nodes from Nutaq [12]. In this paper, we target the programming of picoSDR nodes, but the IPs designed should be portable to other platforms using FPGA, except for the IP implementing the interface between the FPGA and the rest of the board which is usually provided by the board supplier.

One objective of the CorteXlab testbed is to propose open source reference designs as a support for remote experimentation. Particularly it aims at providing :

- Tunable single carrier reference design. We have chosen the Zigbee (802.15.4) standard as defined by IEEE [6]. This is the main contribution of this paper.
- Tunable multiple carrier reference design : SISO/OFDM and MIMO/OFDM which are not presented in this paper.

The software architecture and the room have been selected to target reproducibility and control over the radio propagation and the nodes will have the computing power to run WiFi/LTE in real-time at standard rates and using 2x2 MIMO. The room will contain 22 USRP nodes programmed with GNU radio, 12 2x2 MIMO and 6 4x4 MIMO picoSDR nodes fully integrated and based on a powerful FPGA. Fig. 2 presents the current status of the room: electromagnetic isolation has been performed.

The generic SDR execution model that we target is illustrated on Fig. 3. From our experience, most SDR platform using a FPGA propose a radio control mechanism based on SPI bus, and provide a soft core on the FPGA to handle it. However, it is mandatory to have a direct pipelined data path from the board to the RF front-end in order to take advantage of the maximum throughput available for signal processing data.

Fig. 4 shows the generic architecture of application deployed on Nutaq family of board. The picoSDR uses a similar architecture for PHY layer implementation. Each picoSDR board includes one or two Perseus 6011 advanced mezzanine card, each of which contains a Virtex-6 FPGA connected to two Radio420x RF front-end. The Perseus board contains a Virtex6 FPGA connected on one side to a host processor handling the MAC and application layers and on the other side to the Radio420x front-end. The platform is provided with



Fig. 2: Current status of FIT/CortexLab room, SDR platform will be attached to the roof, the room will have now 50 dB isolation so as to provide reproducible experimental environment.

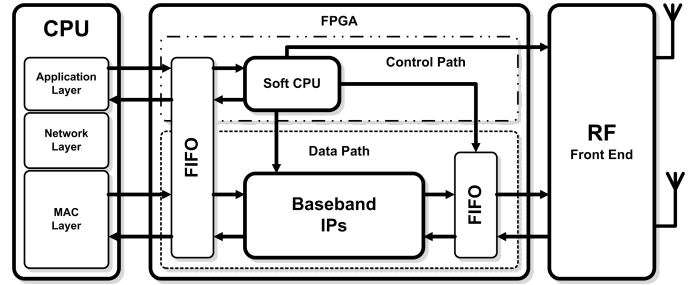


Fig. 3: Targeted SDR platform architecture model, including an FPGA containing a high bandwidth datapath between the CPU and the RF front-end where our IP can be insterted

a reference design that includes a MicroBlaze softCore used for configuration of the radio front-end and a high speed bus named RTDEx (for Real Time Data Exchange). In fact, the key to efficient SDR application is the efficient handling of the data flow between the front-end and the host processor. the core of the baseband processing is performed in the *User logic* IP of Fig. 4, one can see that it is a particular instance of the generic model that we have drawn in Fig. 3. Therefore, the main objective of the Nutaq RTDEx IP core is to provide a framework to exchange data with a host device through the GbE or PCIe links with the highest bandwidth and lower latency possible. In order to avoid any bottleneck in the data throughput, the MicroBlaze processor is bypassed during data packet transmission allowing the full data bandwidth and lower latency due to AXI bus enhanced features compared to the PLB one.

The picoSDR RF front-end is an FPGA Mezzanine Card (FMC) named Radio420X. It is a powerful multimode SDR RF transceiver module designed around the state-of-the-art, multistandard, multiband Lime Microsystems LMS6002D RF transceiver IC. The LMS6002D bandwidth, which is selectable on-the-fly, makes it suitable for a large number of narrowband and broadband applications with excellent channel selectivity. In addition to the integrated analog filters and amplifiers of the LMS6002D RF transceiver, the front end RF card includes external bank of filters and amplifiers that allow better performance.

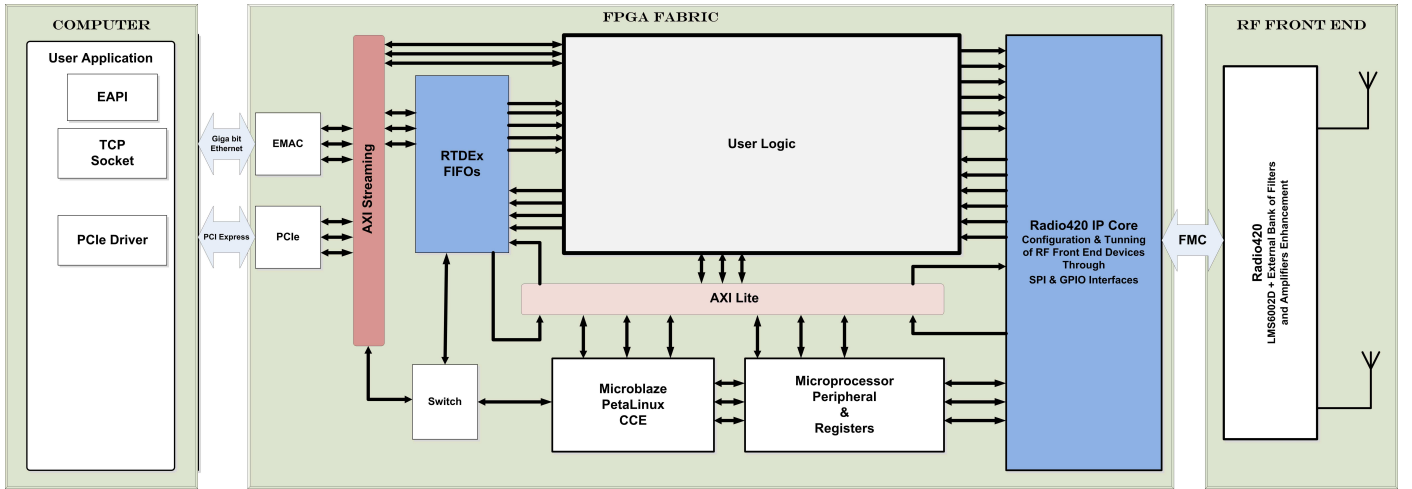


Fig. 4: Nutaq Board Support Development Kit for SDR platforms.

picoSDR platform allows using three design flows: BSDK (Board Support Design Kit), MBDK (Model Based Design Kit) and GNURadio design flow. BSDK is the design flow adopted in the context of CorteXlab testbed to enable HDL design and implementation of open source IPs for SDR systems. The *open* quality refers to the VHDL code we have developed, Nutaq's and Xilinx's IPs provided with the platform (RTDEx bus, EMAC, PCIe, Radio420 Core, etc) are free of charge but not open source of course. The Nutaq Board Software Development Kit (BSDK) is a complete set of tools that includes IP cores, Frameworks, APIs as depicted on the Fig. 4. On top of industry standard board level libraries and APIs, the BSDK includes a complete and efficient transport layer (CCE: Central Communication Engine) that both allows remote control and high speed data exchange between Nutaq FPGA-based hardware and standard processor blades or remote computer.

A typical picoSDR-based design include a MicroBlaze processor instantiated within the FPGA fabric running a commercial embedded Linux distribution named Petalinux. This fabric risk processor runs Nutaq CCE application and may also run user-defined task/application. The CCE handles the bootloader, the start-up sequence, the TCP-IP and PCIe communication and configuration commands, etc. This software component is the board interface with the host Command Line Interpreter, GUIs or any other software running on a remote computer intended to communicate with the Nutaq FPGA-based hardware.

Figure 5 shows the testbed we used for design, implementation, test and validation of the SDR open source IPs. It consists of two picoSDR nodes: the first is a 4x4 node and the second is a 2x2 with an embedded computer. For instance a windows computer is used for HDL coding and synthesizing and another computer with Debian operating system is used for software development of C applications based on Nutaq EAPI.

III. MULTIPLE PHY LAYERS DESIGN & IMPLEMENTATION

This part specifies the hardware TX and RX architectures of IEEE 802.15.4 PHY layers that we have implemented. The complete hardware design has been represented in Fig. 6.

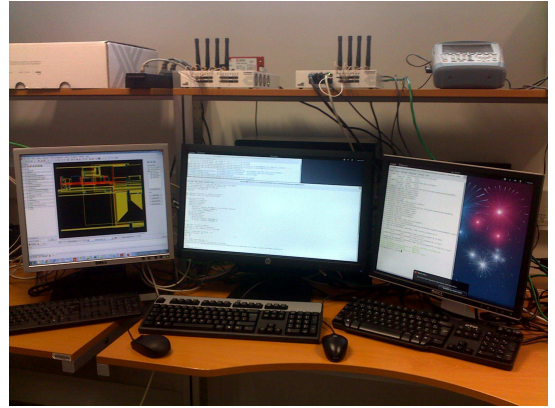


Fig. 5: Development testbed : 2 PicoSDRs and Host machines.

IEEE 802.15.4 standard proposes three options to implement a compliant transmitter [6]. Such a compliant device shall operate in one or several frequency bands using the modulation and spreading formats summarized in Table I. For this, the IP designed should be reconfigurable to adapt to the different parameters (chip rate, frequency band, etc.).

Although IEEE 802.15.4 standard is intended to conform with established regulations in Europe, Japan, Canada, and the United States, CorteXlab testbed is shielded and electromagnetically isolated environment that allows users to experiment all the options regardless of regulatory constraints. One can even transmit and receive at any frequency in the range of 0.3 - 3.8 GHz. Thus, this unique feature will help to extend the experimentation use cases and enable exploration of further opportunities to enhance wireless communication technologies.

Naturally according to Table I, option 1 and option 2 physical layer specifications are slightly the same except the chip and the symbol rates. For this reason they are represented by the same IP which can be configured to run in mode 1 or mode 2 by simply changing the input clock. The latter is performed through a software reconfiguration that easily

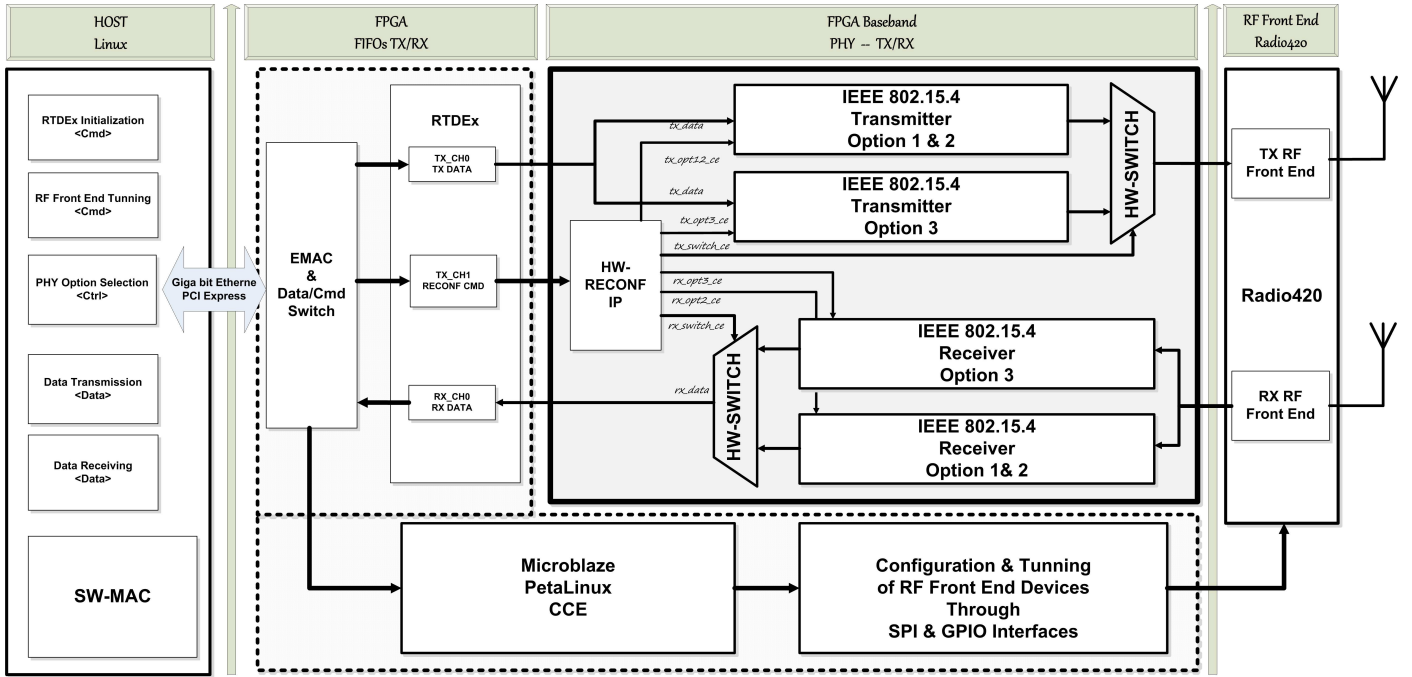


Fig. 6: Block diagram of our multiple PHY layers implementation of the IEEE 802.15.4 standard.

TABLE I: IEEE 80.15.4 PHY Layer Specifications.

PHY Option	Frequency Band (MHz)	Spreading Parameters			Modulation	Data Parameters			Filter Parameters
		Chip rate (kcps)	Spreading Sequence Length	Number of Sequence		Bit rate (kbps)	Symbol rate (kips)	Symbols	
Option 1	868-868.6	300	16	2	BPSK	20	20	Binary	Raised Cosine Filter
Option 2	902-928	600	16	2	BPSK	40	40	Binary	Raised Cosine Filter
Option 3	2400-2483.5	2000	32	16	O-QPSK	250	62.5	16-ary Orthogonal	Half-Sine Filter

modify the design clock provided by the PLL of the Radio420x transceiver. Hence, we greatly minimize the FPGA resources needed to map this multiple mode design.

Nevertheless, option 3 physical layer specifications are extremely different from those of option 1 and option 2. Furthermore, option 3 physical layer specifications are more complex to design and implement in hardware. Hence it is natural to provide a hardware switch IP to switch between option 1/2 and option 3 IPs as illustrated in Fig. 6. The baseband IP (shaded on Fig. 6) is plugged to a dedicated FIFO of the RTDEx bus (in the case of implementation on picosDR) and it communicates with a software API running on the host. The latter sends the user choice (option 1/2 or 3) to the HW switch through Gigabit Ethernet or PCI Express link to enable the suitable IP accordingly.

In the same way as the transmitting path of the multiple layers implementation of the IEEE 802.15.4 standard, the receiving path contains two receivers each one of them performs data reception and decoding according to the enabled option. The switching process is controlled by a Finite State Machine that enables one of those receivers and configure the switch to

output the expected stream as illustrated in the Fig. 6. One can see in this figure the software tasks that should be performed on the computer side such as RTDEx initialization, RF front-end tuning, PHY option selection, data transmission and reception. Therefore, in parallel to the baseband IPs the FPGA fabric instantiate the Microblaze softCore running the CCE (central communication engine) and other IP cores used to configure the RTDEx bus, to tune and to perform the suitable connection with the RF front-end devices.

In the next subsections, we consider the transmitter and the receiver architectures of the physical layer, first for option 1 and 2, then for option 3.

A. TX Architecture

In this section we present the baseband architecture of the IEEE 802.15.4 transmitters we implemented in this work. The IEEE standard [6] indicates how to form the frame, and the performance that should be obtained by the receiver, but does not specify exactly how the receiver should be implemented. Hence, it is much more open and difficult to implement the receiver part. In particular synchronization mechanism has to

be carefully designed, this is one of the contribution of this paper.

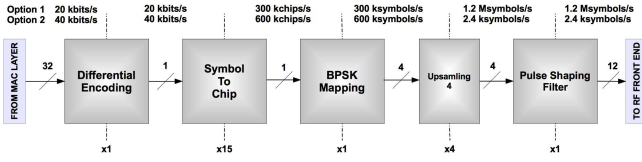


Fig. 7: Block diagram of IEEE 802.15.4 option 2 Transmitter.

1) *TX architecture of PHY Layer Option 1 & 2:* The data rates of options 1 and 2 are respectively 20 kb/s and 40 kb/s. Both of option 1 and 2 use direct-sequence spread spectrum (DS-SS) with binary phase-shift keying (BPSK) used for chip modulation and differential encoding used for data symbol encoding. Each input bit shall be mapped into a 15-chip pseudo-random sequence as specified in Table II.

TABLE II: IEEE 80.15.4 Option 1& 2 symbol-to-chip mapping.

Input symbol (bits)	Chip values $c_0 c_1 \dots c_{14}$
0	111101011001000
1	000010100110111

The block diagram of the TX chain is provided in Fig. 7, it basically corresponds to the corresponding IP implemented. The IEEE 802.15.4 frame arrives splitted in 32 bit word from the RTDEX FIFO bus, each bit is encoded with respect to the previous bit in the differential encoding IP. The symbol to chip IP multiply the sample rate by 15 using table II. Modulation is performed using BPSK, then upsampling and pulse shaping are performed before digital to analog conversion which is performed in the RF front-end.

Configuration switching between Option 1 and 2 is simply done by reconfiguring the design clock provided by the PLL of the RF front-end. This reconfiguration process uses the Nutaq API to send a command with the sampling frequency of the ADC and DAC to the CCE through the gigabit ethernet link. The CCE running on the MicroBlaze SoftCore decodes the value of the sampling frequency and uses it to configure the PLL on the Radio420x through an SPI interface. This configuration allows the generation of the reference clock of the baseband IPs which is two times the sampling frequency.

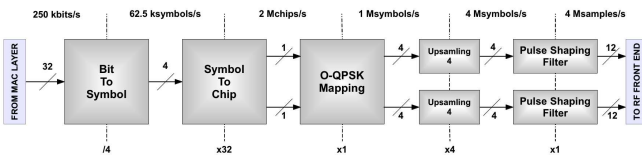


Fig. 8: Block diagram of IEEE 802.15.4 option 3 Transmitter

2) *TX architecture of PHY Layer Option 3:* The specification of the third option of IEEE 802.15.4 PHY layer

supports data rate of up to 250kb/s. It uses DS-SS with O-QPSK (offset quadrature phase shift keying) as modulation type. Each O-QPSK symbol is one of 16 orthogonal pseudo-random sequences. Each symbol is 32 chip long and corresponds to one of 16 possible combinations of four bits as partly depicted in Table III. The resulting chip rate is 2 Mchips/s. Fig. 8 illustrates a typical block diagram of the implemented IP of a transmitter conform to the option 3 specifications.

TABLE III: IEEE 80.15.4 Option 3 symbol-to-chip mapping.

Data symbol $(s_k)_{10}$	Data symbol $(s_k)_2$	Chip values $c_0 c_1 \dots c_{31}$
0	0000	11011001110000110101001000101110
1	0001	11101101100111000011010100100010
2	0010	00101110110110011100001101010010
...		
14	1110	10010110000001110111101110001100
15	1111	11001001011000000111011110111000

B. RX Architecture

As indicated in Fig. 9, a typical digital receiver receives the digitized complex baseband signal from RF front-end transceiver. Then it applies a matched filter in order to maximize the signal to noise ratio (SNR). The received signal contains not only the data symbols that should be decoded but also unknown parameters such as frequency and phase offsets and the sampling time. Therefore, an accurate estimation of these parameters is vital for reliable data detection. The discussion below outlines some possible methods for estimating carrier offset and sampling time. Once the compensation for distortion and timing recovery are performed, the gathered symbols are then processed by a detector. Detection processing can be a very simple device that makes decision of either a symbol is 0 or 1. However, in communication standards data are formatted in a specific way to help easy decoding procedure as it is the case of IEEE 802.15.4 standard. For instance, preamble and start of frame delimiter (SFD) are added to the frame to help symbol time synchronization and enable the data decoding. Thus, the detector module of Fig. 9 must perform complex baseband processing including preamble correlation, SFD correlation, and a bank of symbol correlators to detect the correct symbols as it will be outlined later in this section.

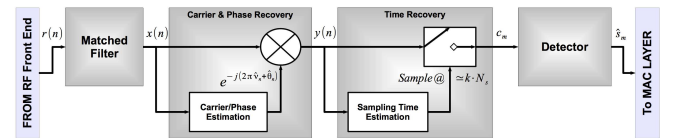


Fig. 9: Block diagram of a coherent receiver.

This section will provide a useful and understandable way to implement most of the receiver functionalities such as energy detection, carrier and phase recovery, clock recovery, symbol correlation, preamble correlation, SFD correlation, etc. The receiver is also duplicated for option 1/2 and option 3. In fact, we implemented two receivers one for each option as illustrated in Fig. 6. Those receivers share the same structure

as illustrated in Fig. 9. However, they are little bit different from an implementation point of view since in the case of option 3 the baseband digital processing is performed on both I and Q signals whereas in the case of option 1/2 BPSK modulated signal is simple to demodulate. For instance, the major difference between the two receivers is naturally the decoder IP where massive correlations are performed to detect the preamble and the SFD in addition to decoding procedure of symbols.

Fig. 10 presents our implementation of option 3. The *detector* bloc includes two correlators, one used for preamble detection and the other used for frame delimiter detection, a small controller (FSM for finite state machine), and the symbol bank correlation. The symbol bank correlation is in charge of comparing blocs of 32 chips against data symbol in a bank to recover the coded data symbols (reverse work as the one presented in table III). Before that, the frame has to be synchronized. When the FSM is informed by the preamble correlation IP that a preamble has been detected, it launches the start frame delimiter detection (SFD correlation). When SFD is detected, data are send bloc by bloc to the symbol bank correlator.

The rest of the section focus on the implementation of synchronization and correlation functions in the receiver which are the main technical difficulties of this IP.

1) *Carrier and Phase Recovery*: In a typical wireless communication system, imperfect up-conversion and down-conversion caused by non-ideal transmitter and receiver local oscillators result in a carrier offset at the receiver. This offset causes a continuous rotation of the signal constellation, and must be corrected in order to achieve reliable demodulation of the received signal.

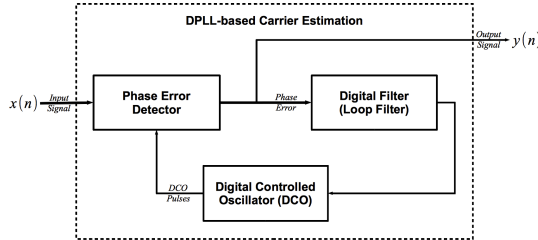


Fig. 11: Basic block diagram of a Digital Phase Locked-Loop (DPLL) used for carrier offset

There are many ways to implement carrier synchronization in a digital communication system. We present here a method that tune together the frequency and phase, hence carrier and phase are simultaneously recovered. At the heart of all synchronizers is the phase-locked loop (PLL). A basic block diagram is shown in Fig. 11. This DPLL consists of three modules : the phase detector, the loop filter and the digital controlled oscillator. It employs proportional and integral loop filters formed by a scaled digital integrator and a scaled direct path. The filter coefficients control the PLL bandwidth and damping factor. In the PLL digital implementation, the DCO takes the form of a direct digital synthesizer (DDS). The phase detector can be implemented using the arctangent operation which can be performed by a CORDIC IP in vectoring mode [1].

The schematic view of the DPLL IP we implemented is given in Fig. 12. It contains a phase detector, an error generator and a loop filter. The purpose of the phase detector and DCO is to detect the phase of the input signal then rotate it by the estimated phase at the output of the loop filter. Therefore, those functions (of the Phase detector and the DCO) can be combined and simply implemented by a CORDIC module in rotation mode as illustrated in Fig. 12. In the next section we will present the functional description of the CORDIC algorithm in rotation mode and we will describe some aspects related to its HDL implementation.

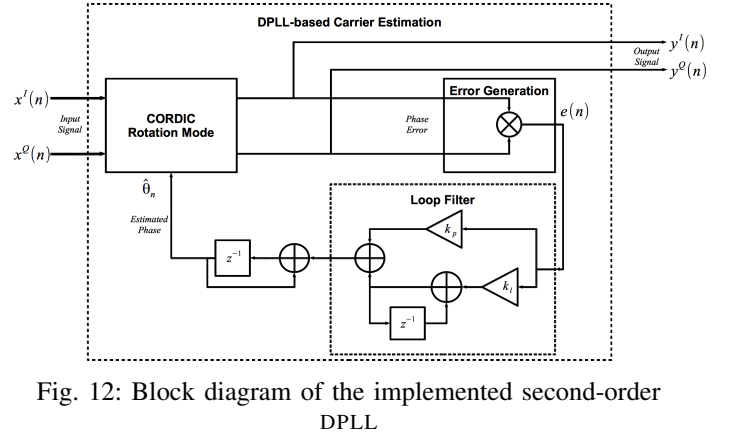


Fig. 12: Block diagram of the implemented second-order DPLL

a) *CORDIC in Rotation Mode*: In the rotation mode, the angle accumulator is initialized with the desired rotation angle. The rotation decision at each iteration is made to diminish the magnitude of the residual angle in the angle accumulator. The decision at each iteration is therefore based on the sign of the residual angle after each step. For rotation mode, the CORDIC equations are [1] :

$$\begin{aligned} x_{i+1} &= x_i - y_i \cdot d_i \cdot 2^{-i} \\ y_{i+1} &= y_i - x_i \cdot d_i \cdot 2^{-i} \\ z_{i+1} &= z_i - d_i \cdot \tan^{-1}(2^{-i}) \end{aligned}$$

where

$$d_i = -1 \quad \text{if } z_i < 0, +1 \quad \text{otherwise}$$

which provide the following result :

$$\begin{aligned} x_n &= A_n \cdot (x_0 \cdot \cos z_0 - y_0 \cdot \sin z_0) \\ y_n &= A_n \cdot (y_0 \cdot \cos z_0 + x_0 \cdot \sin z_0) \\ z_n &= 0 \\ A_n &= \prod_{i=1}^n \sqrt{1 + 2^{-2i}} \end{aligned}$$

The CORDIC algorithm can be implemented either in an iterative way or as a pipelined architecture. Iterative CORDIC implementation takes more than a clock cycle for each output value. It is useful when the FPGA resources are limited and the

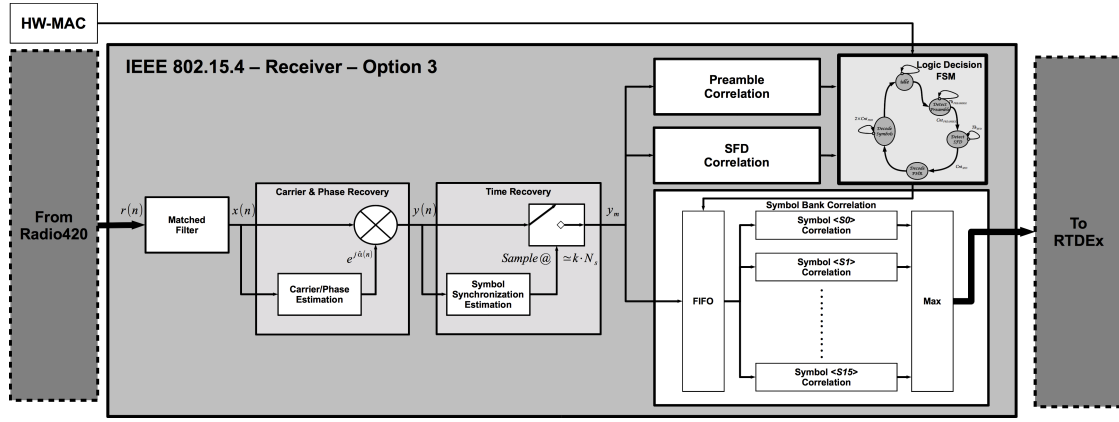


Fig. 10: Block diagram of IEEE 802.15.4 option 3 Receiver

design speed is not high. However, pipelined implementation provides an output values each clock cycle after pipeline stages propagation. Therefore, it is more suited for high speed design. Nevertheless it takes more FPGA resources than the iterative CORDIC implementation.

In order to reduce the number of clock cycle, the pipelined CORDIC architecture was implemented and it uses a generic number of stages. For better performance, a 16-stages pipelined CORDIC was synthesized to make accurate phase rotation in the DPLL IP.

2) *Symbol Timing Recovery*: There exist different way and techniques allowing time recovery such as Mueller and Müller [9], Gardner [5], Early-Late-Gate algorithms (ELG) [14]. In the case of our implementation ELG algorithm is used to find optimal sample instance of the chip. Fig. 13 shows the structure of block diagram of the ELG algorithm. It consists of three main sub-blocks : 1- the absolute value of the real part of the input signal, 2- a down sampling module controlled by the decision logic unit which is the third sub-block.

The sampling control block, which is based on a digital implementation of the classical early-late gate technique[14] adjusts the sampling instant to move towards the peak or dithers around the peak if it has already been found. The operation of the early-late gate synchronizer is explained in [14], the functional description of the theory behind the early late gate algorithm can be found in the authors paper [2]. The algorithm found here is modified with respect to the original version. In fact the insertion of the real part operator is made to allow O-QPSK (Option 3) to be included.

3) *Decoder*: The proposed decoder performs three levels of correlation to detect the preamble, the start of frame delimiter (SFD) and symbols. Therefore, a FSM was implemented to control this complex hardware processing. If the preamble correlation is greater to some threshold, the FSM moves to SFD correlation state and compares the correlation to a certain threshold to determine if an IEEE 802.15.4 packet was actually present or not. If a valid packet was detected, the FSM moves to symbol decoding state and enable the bank of symbol correlator to perform parallel correlations and pick up the index of the symbol correlator that gives the highest correlation value as illustrated in Fig. 10.

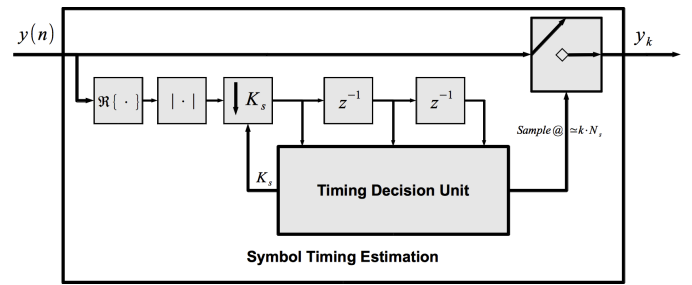


Fig. 13: Bloc diagram of timing estimation module implementing the early-late-gate algorithm.

Naturally, the decoder consists of many instances of correlators which have in common a correlation algorithm. The latter can be mathematically formulated as follows :

$$C_{cy}(n) = \sum_{k=0}^{N-1} c(k) \cdot y(n-k) \quad (1)$$

Where N is the number of chips in the spreading sequence, c is the spreading reference sequence, and y is the received signal after carrier/phase recovery and timing synchronization. Both c and y samples are NRZ encoded using 1 bit to maximize the correlation value.

From now we will consider only the decoder description of the option 3 PHY layer specifications to illustrate how its IPs are implemented. The same structure was implemented for option 1 and 2 PHY layer with lower complexity because of BPSK modulation.

Preamble and SFD correlations are performed on complex baseband signals at the chip level for 1 byte of data. The correlator structure is illustrated in Fig. 14. It consist of two reference sequences representing the I and Q components, two long shift registers to memorize the I and Q chips, a matrix of multipliers, and a sum module to compute the I and Q correlation values according to formula (1). For instance, complex operations were added to compute the real and the imaginary parts of the correlation product. Finally, the square

of the module of the complex correlation value is calculated as shown in Fig. 14.

In order to reduce the number of propagation cycles a tree topology of 15 comparators was implemented to pick up the index of the symbol correlator which have the maximum correlation value. In fact, the index of each correlator is a 4 bit binary code that matches a unique 32 bits spreading sequence according to the table III for the option 3 PHY layer. A structure view of the implemented symbol bank correlator and the tree topology of comparators to find maximum value of correlation that match the decoded symbol is illustrated in Fig. 15.

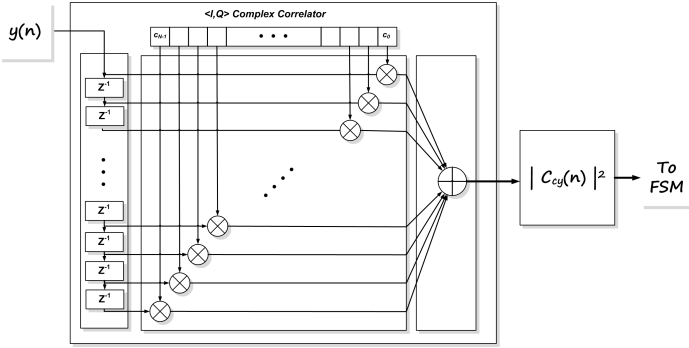


Fig. 14: Bloc diagram of the hardware implementation of the correlation algorithm.

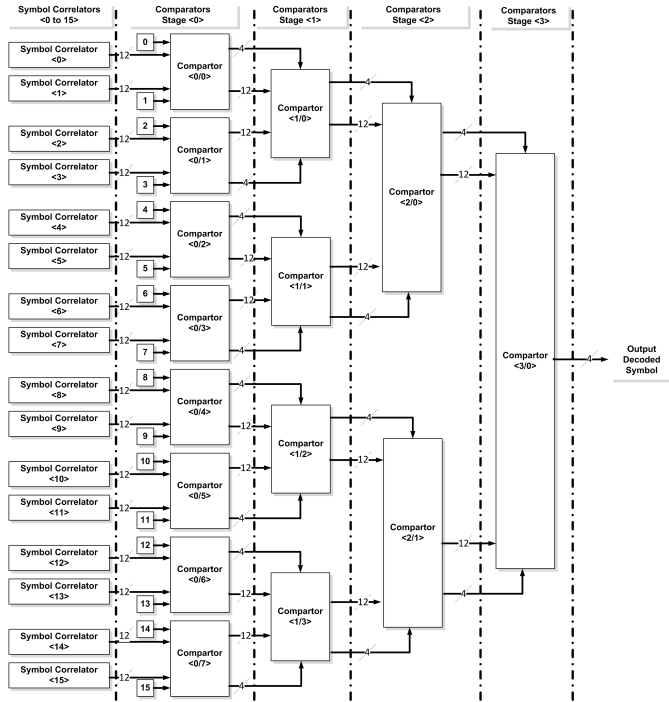


Fig. 15: Structure view of the implemented symbol bank correlator and the tree topology of comparators to find maximum value of correlation that match the decoded symbol.

IV. IMPLEMENTATION RESULTS

This section presents the performance of the IPs implemented. Table IV gives a summary of the resource utilization spent by our IEEE 802.15.4 IPs on the Xilinx FPGA. Tables V and VI present a detailed description of resource utilization for transmitter option 1/2 and option 3 IPs while Table VII and VIII present resource utilization for the receivers for both option 1/2 and option 3. One can see that Table VII for option 1/2 does not contain all the IPs of the proposed architecture. This is simply due to the fact that many modules are shared between both options. Therefore, to avoid duplication of results we presented the resource utilization for the shared modules only in the Table VIII related to option 3 receiver.

As already explained, the design has been implemented on Nutaq picosDR platform which is based on the Perseus 6011 digital domain board with a Virtex-6 XC6VSX315T FPGA. Our contribution consists in the design of a multiple PHY layers design of the IEEE 802.15.4 standard, in addition to the TX and RX IPs, the FPGA fabric contains a Microblaze processor running a PetaLinux operating system aimed to configure EMAC, EDMA and RTDEX busses and to tune the RF Front-End Radio420 transceiver.

The design methodology was the following: a first Matlab version of the TX and RX flow was functionally validated by Matlab simulation. Then, the IPs were written in register transfer level VHDL, different clock rate could be obtained with a systematic clock enable input for each IP. The net listing process of the IPs was done on Xilinx Platform Studio (XPS), the synthesis place and route were done with Xilinx Synthesis Technology (XST). Simulation was first realized with matlab version of each IP, then the VHDL was simulated using Modelsim and checked with chipscope.

The total *user logic* IP (i.e. the shaded area on Fig. 6) uses less than 5% of the FPGA. According to table VII we can notice that most of the resource are spent by the receiver. We can observe also that DSP48 resources are mainly used as multipliers to compute energy of preamble, SFD, and symbols inside the decoder. The proposed multiple layer implementation of the IEEE 802.15.4 standard requires only fewer number of slices and multipliers compared to the available resources and it does not make use of Block-RAM memories which can be left to more complex design. The higher clock frequency that can be achieved by the implemented IPs is up to 200 MHz. Whereas, as explained before, the input clock of this design is provided by the Radio420 front-end receiver in the case of picosDR node where the maximum sampling frequency is 40 MHz. Therefore, our design can run at least at 80 MHz or higher frequency complying to Shannon theorem. Furthermore, it can be used with RF front-end transceiver which had larger bandwidth up to 100 MHz.

The resource utilization of the implemented IPs shows that designers can think to parallel implementation of much more complex SDR designs on FPGA such as single and multiple carrier baseband communication systems and MIMO processing.

V. CONCLUSION

The continuing need for high data rate RF technologies and cognitive radio systems pushed a very wide research activities

TABLE IV: Device Utilization Table Summary.

IP Core	Logic Utilization	Used	Available	Utilization
Transmitter Option 1 & 2	Slice Registers	150	393600	0.038%
	Slice LUTs	140	196800	0.071%
	Occupied Slices	72	49200	0.146%
Transmitter Option 3	Slice Registers	269	393600	0.068%
	Slice LUTs	230	196800	0.117%
	Occupied Slices	115	49200	0.234%
Receiver Option 1 & 2	Slice Registers	1499	393600	0.381%
	Slice LUTs	1709	196800	0.868%
	Occupied Slices	652	49200	1.325%
	DSP48s	23	1344	1.711%
Receiver Option 3	Slice Registers	1879	393600	0.477%
	Slice LUTs	1758	196800	0.893%
	Occupied Slices	697	49200	1.417%
	DSP48s	57	1344	4.241%
IEEE 802.15.4 TX/RX total	Slice Registers	3797	393600	0.964%
	Slice LUTs	3837	196800	1.949%
	Occupied Slices	1536	49200	3.122%
	DSP48s	80	1344	5.958%

TABLE V: Device Utilization Table Summary of the option 1 and 2 transmitter.

IP Core	Logic Utilization	Used	Available	Utilization
SERDES 32 to 1	Slice Registers	73	393600	0.019%
	LUTs	69	196800	0.035%
	Occupied Slices	28	49200	0.057%
Tx Clock Generator	Slice Registers	11	393600	0.003%
	LUTs	31	196800	0.016%
	Occupied Slices	9	49200	0.018%
Differential Encoder	Slice Registers	1	393600	0.000%
	LUTs	1	196800	0.001%
	Occupied Slices	1	49200	0.002%
Bit to Chip	Slice Registers	9	393600	0.002%
	LUTs	7	196800	0.004%
	Occupied Slices	5	49200	0.010%
BPSK Mapping	Slice Registers	0	393600	0.000%
	LUTs	1	196800	0.001%
	Occupied Slices	1	49200	0.002%
Tx Filter RRCF	Slice Registers	27	393600	0.007%
	LUTs	58	196800	0.029%
	Occupied Slices	21	49200	0.043%
IQ MUX LMS6002D	Slice Registers	40	393600	0.010%
	LUTs	26	196800	0.013%
	Occupied Slices	11	49200	0.022%

to enhance SDR communication systems. Up to very recently, SDR technology was only accessible to restricted communities and nowadays, it becomes more and more affordable. In addition, FPGAs provide flexibility to achieve SDR signal processing and RF tuning, simultaneously with high levels of performance and cost efficiency. Even if GNUradio community is opening-up new opportunities to implement SDR design, there is still further needs to make open source hardware designer to re-use their own IPs for digital-up and digital-down conversion. Therefore, new SDR and cognitive radio testbeds should give an open access supported with open source HDL design for scientific community. This is the main objective of *CorteXlab* testbed in which context the present work is carried out.

This paper has provided an tutorial approach of how the baseband part of IEEE 802.15.4 standard can be implemented on FPGA target. A multiple PHY layer design was presented to allow experimentation, in *CorteXlab* testbed, of all the possibilities offered by the standard regardless of regulatory

TABLE VI: Device Utilization Table Summary of the option 3 transmitter.

IP Core	Logic Utilization	Used	Available	Utilization
Bit to Symbol	Slice Registers	74	393600	0.019%
	LUTs	65	196800	0.033%
	Occupied Slices	21	49200	0.043%
Tx Clock Generator	Slice Registers	16	393600	0.004%
	LUTs	22	196800	0.011%
	Occupied Slices	7	49200	0.014%
Symbol to Chip	Slice Registers	73	393600	0.019%
	LUTs	63	196800	0.032%
	Occupied Slices	23	49200	0.047%
O-QPSK Mapping	Slice Registers	7	393600	0.002%
	LUTs	5	196800	0.003%
	Occupied Slices	6	49200	0.012%
Tx Filter I Path	Slice Registers	27	393600	0.007%
	LUTs	59	196800	0.030%
	Occupied Slices	23	49200	0.047%
Tx Filter Q Path	Slice Registers	27	393600	0.007%
	LUTs	59	196800	0.030%
	Occupied Slices	23	49200	0.047%
IQ MUX LMS6002D	Slice Registers	64	393600	0.016%
	LUTs	50	196800	0.025%
	Occupied Slices	24	49200	0.049%

limits. The design flow and the proposed architecture are generic and hence they can be applied to implement an FPGA-based single carrier communication system on Nutaq and other SDR platforms with minor adaptations. We have presented the FPGA resources occupied by the proposed IPs (less than 5% of the FPGA all together). These IPs can be re-used by designers to build an open source HDL library for SDR systems.

As short term perspectives to the proposed receiver architectures, we plan to add an LQI (stands for Link Quality Indication) IP which purpose aims to compute a measurement characterizing the strength and/or quality of a received packet. This measurement may be implemented using receiver ED (Energy Detection), a signal-to-noise ratio estimation, or a combination of these methods. The LQI IP should help performing tests of ACM-based (for Adaptive Coding & Modulation) scenario where modulation switching criteria is based on continuous estimation and monitoring of SNR. This will allow the system to switch PHY options before errors are detected by the user. Besides, to make our multiple layer HDL implementation fully compatible with the IEEE 802.15.4 standard, a MAC layer must be co-designed and implemented on both FPGA and the host machine. Currently, we have a very light MAC layer that performs packet building and we are studying the adaptation of TKN15.4, Open-ZB or OpenMAC which are open-source implementations of the IEEE 802.15.4/ZigBee protocol stack targeted tinyos platforms.

Finally, in the context of *CorteXlab* testbed development, future work will focus on multiple carrier and multiple antenna systems which will bring more open-source design to scientific community. This will enable more understanding of FPGA implementation of baseband blocks of PHY layer and will take advantage of the open access to *CorteXlab* testbed to test and develop new design while reusing available IPs.

REFERENCES

- [1] R. Andraka, "A survey of cordic algorithms for fpga based computers," in *Proceedings of the 1998 ACM/SIGDA sixth international symposium*

TABLE VII: Device Utilization Table Summary of the option 3 receiver.

IP Core	Logic Utilization	Used	Available	Utilization
IQ DEMUX LMS6002D	Slice Registers	64	393600	0.016%
	LUTs	50	196800	0.025%
	Occupied Slices	24	49200	0.049%
Rx Matched Filter (8 Taps) I Path	Slice Registers	264	393600	0.067%
	LUTs	116	196800	0.059%
	Occupied Slices	58	49200	0.118%
	DSP48s	8	1344	0.595%
Rx Matched Filter (8 Taps) Q Path	Slice Registers	264	393600	0.067%
	LUTs	116	196800	0.059%
	Occupied Slices	58	49200	0.118%
	DSP48s	8	1344	0.595%
CORDIC ROTATION MODE (DPLL)	Slice Registers	74	393600	0.019%
	LUTs	65	196800	0.033%
	Occupied Slices	21	49200	0.043%
Error Generator DPLL	Slice Registers	73	393600	0.019%
	LUTs	63	196800	0.032%
	Occupied Slices	23	49200	0.047%
	DSP48s	1	1344	0.074%
Loop Filter DPLL	Slice Registers	7	393600	0.002%
	LUTs	5	196800	0.003%
	Occupied Slices	6	49200	0.012%
	DSP48s	2	1344	0.149%
Carrier Phase Recovery	Slice Registers	773	393600	0.196%
	LUTs	1071	196800	0.544%
	Occupied Slices	343	49200	0.697%
	DSP48s	3	1344	0.223%
CORDIC VECTORING MODE	Slice Registers	565	393600	0.144%
	LUTs	1014	196800	0.515%
	Occupied Slices	312	49200	0.634%
Preamble & SFD Correlator	Slice Registers	34	393600	0.009%
	LUTs	18	196800	0.009%
	Occupied Slices	17	49200	0.035%
	DSP48s	2	1344	0.149%
Symbol Correlator	Slice Registers	34	393600	0.009%
	LUTs	18	196800	0.009%
	Occupied Slices	13	49200	0.026%
	DSP48s	2	1344	0.149%
Bank of Symbol Correlator	Slice Registers	429	393600	0.109%
	LUTs	339	196800	0.172%
	Occupied Slices	161	49200	0.327%
	DSP48s	32	1344	2.381%
FSM for Decoder	Slice Registers	4	393600	0.001%
	LUTs	8	196800	0.004%
	Occupied Slices	5	49200	0.010%
Decoder	Slice Registers	456	393600	0.116%
	LUTs	335	196800	0.170%
	Occupied Slices	180	49200	0.366%
	DSP48s	36	1344	2.679%

TABLE VIII: Device Utilization Table Summary of the option 1 & 2 receiver.

IP Core	Logic Utilization	Used	Available	Utilization
Preamble & SFD Correlator	Slice Registers	6	393600	0.002%
	LUTs	6	196800	0.003%
	Occupied Slices	4	49200	0.008%
	DSP48s	1	1344	0.074%
Symbol Correlator	Slice Registers	33	393600	0.008%
	LUTs	95	196800	0.048%
	Occupied Slices	31	49200	0.063%
Bank of Symbol Correlator	Slice Registers	60	393600	0.015%
	LUTs	266	196800	0.135%
	Occupied Slices	122	49200	0.248%
FSM for Decoder	Slice Registers	4	393600	0.001%
	LUTs	8	196800	0.004%
	Occupied Slices	5	49200	0.010%
Decoder	Slice Registers	76	393600	0.019%
	LUTs	286	196800	0.145%
	Occupied Slices	135	49200	0.274%
	DSP48s	2	1344	0.149%

IEEE, vol. 27, no. 3, pp. 159–167, 2010.

- [8] J. Mitola III, “The software radio,” in *IEEE National Telesystems Conference*, 1992.
- [9] K. H. Mueller and M. Müller, “Timing recovery in digital synchronous data receivers,” *IEEE Transactions on Communications*, vol. 24, pp. 516–531, 1976.
- [10] “Universal software radio peripheral (USRP),” <http://www.ettus.com>, National Instrument.
- [11] T. Newman, S. Shajedul Hasan, D. DePoy, T. Bose, and J. Reed, “Designing and deploying a building-wide cognitive radio network testbed,” *Communications Magazine, IEEE*, vol. 48, no. 9, pp. 106–112, 2010.
- [12] “PicoSDRmake cognitive radio,” <http://nutaq.com/en/products/picosdr>, Nutaq.
- [13] “OpenCores: Open source hardware IP cores,” <http://opencores.org>, OpenCores.
- [14] J. G. Proakis, *Digital Communications*, 4th ed. McGraw-Hill, 2000.
- [15] A. Sanchez, I. Moerman, S. Bouckaert, D. Willkomm, J. Hauer, N. Michailow, G. Fettweis, L. Dasilva, J. Tallon, and S. Pollin, “Testbed federation: an approach for experimentation-driven research in cognitive radios and cognitive networking,” in *Future Network & Mobile Summit (FutureNetw)*, 2011. IEEE, 2011, pp. 1–9.
- [16] P. Steenkiste, D. Sicker, G. Minden, and D. Raychaudhuri, “Future Directions in Cognitive Radio Network Research,” 2009, nSF Workshop Report.

on Field programmable gate arrays, New York, NY, USA, 1998, pp. 191–200.

- [2] K.-C. Chen and J.-M. Lee, “A family of pure digital signal processing bit synchronizers,” *IEEE Transactions on Communications*, vol. 45, no. 3, pp. 289–292, 1997.
- [3] M. Dardaillon, K. Marquet, T. Risset, and A. Scherrer, “Software Defined Radio Architecture Survey for Cognitive Testbeds,” in *Wireless Communications and Mobile Computing Conference (IWCMC)*, 2012 8th International, Limassol, Cyprus, Sep. 2012.
- [4] “Equipex FIT: Future Internet of Things,” <http://fit-equipex.fr>, French National Research Agency, ANR.
- [5] F. M. Gardner, “Interpolation in digital modems. I. Fundamentals,” *Communications, IEEE Transactions on*, vol. 41, no. 3, pp. 501–507, Aug. 1993.
- [6] “Part 15.4: Wireless Medium Access Control (MAC) and Physical Layer (PHY) Specifications for Low-Rate Wireless Personal Area Networks (WPANs),” IEEE Computer Society, 2006, IEEE Std 802.15.4-2006.
- [7] M. Mattavelli, I. Amer, and M. Raulet, “The reconfigurable video coding standard [standards in a nutshell],” *Signal Processing Magazine*,